Side Forces on Ogive-Cylinder Bodies at High Angles of Attack in Transonic Flow

GEORGE S. PICK*
Naval Ship Research and Development Center, Bethesda, Md.

Theme

AN experimental investigation is reported involving side force measurements on ogive-cylinder bodies for a family of nose geometries. Results are presented at the $M = 0.5$ to 1.1 range for angles of attack between 15 and 45° involving both laminar and turbulent boundary layers.

Content

Flow characteristics about slender axisymmetric bodies of revolution at high angles of attack in the high subsonic and transonic speed range are poorly understood. This may be ascribed to several extremely complex interactions involving inviscid mixed subsonic and supersonic flows, viscous attached and separated boundary-layer flow, and the resulting vortex flow. It was reported in Ref. 1 that at high subsonic and transonic flows and at angles of attack above 20°, with zero side-slip, ogive-cylinder bodies of revolution exhibited rather large steady side forces. The direction and magnitude of these side forces were unpredictable. Pressure distribution measurements and schlieren photographs in Ref. 2 indicated that an unsymmetric vortex buildup was causing these forces. In spite of reported failures in various research programs due to unexpected side forces, no systematic data exist which deal with physical causes or effects. Consequently, the objective of the present investigation was to obtain systematic information about the effects of Mach number, nose geometry, angle of attack, and boundary layer conditions on the measured side forces.

The experiments were conducted in the NSRDC 18-in. indraft tunnel using a slotted test section. Unit Reynolds numbers varied between 2.7×10^6/ft and 4.3×10^6/ft for the speed range of $M = 0.5$–$M = 1.1$ (0.5, 0.6, 0.7, 0.8, 0.9, and 1.1). Tangent ogive noses of fineness ratios (F.R.) 2, 3, and 4 were tested with bluntness ratios (B.R.) of 0 to 50% (100 nose tip radius/base radius) using a cylindrical afterbody of 1.1 in. base diameter and 8.688 in. length. Schematic diagram of the tested configurations are shown in Fig. 1. Aerodynamic forces were obtained by a six component internal balance. Schlieren photography and oil flow techniques provided both external and surface flow visualization. At several speeds, roll angles were changed from 0–90° and 180° to check the flow sensitivity to small geometric changes. At $M = 0.5$, 0.7, and 0.9, both laminar and turbulent boundary layers were examined. Turbulent boundary layers were generated by a $\frac{1}{8}$ in. wide strip of No. 54 Grit placed from the nose to the base of the models along the windward meridian.

The flow model which can be reconstructed from the schlieren photographs, oil flow experiments and aerodynamic force measurements is in general agreement with the crossflow theory developed in Ref. 3. At $\alpha < 20°$, two symmetrical vortex sheets are generated which feed from the separated boundary layer and stay parallel to the body axis. At higher angles of attack ($\alpha < 25°$), the adverse pressure gradient, combined with slight geometric irregularities in the nose tip region, causes one vortex sheet to stop growing and forces it to depart from the surface. The other vortex sheet stays attached for a while longer and eventually departs from the surface. As the angle of attack increases, the number and strength of the shed vortices increase. The strength of these vortices are not equal. This stems from the fact that the vortex strength is proportional to the breakaway point location (g, measured along the body axis from the nose tip) which can be expressed as:

$$\Gamma/V_\infty \, d \sin \alpha = 0.8348(g/d) \tan \alpha \qquad (1)$$

(Γ vortex strength, V_∞ freestream velocity, d afterbody diameter). The difference in vortex strength and the misalignment of the freestream velocity vector and shed vortex sheets account for the direction and magnitude of the side forces.

The initial direction of the asymmetric vortex paths is unpredictable, since it is due to the random geometric nose tip irregularities. Correspondingly, the initial direction of the side force is not predictable, However, once the direction is established, it tends to remain as the incidence angle is increased. The change in roll angle causes the nose irregularities to roll with the model and this in turn alters the sign and, to a lesser degree, the magnitude of the side forces. The measured side forces remain small below $\alpha = 25°$. Beyond this, they increase and reach their peak at around 35 to 40°. In general, as the Mach number increases, the side force coefficient (C_Y)† decreases within the experimental envelope. Typical examples are shown in Fig. 2. In all tested Mach numbers, the magnitude of the average side forces increased with increasing fineness ratio. This again is demonstrated in Fig. 2.

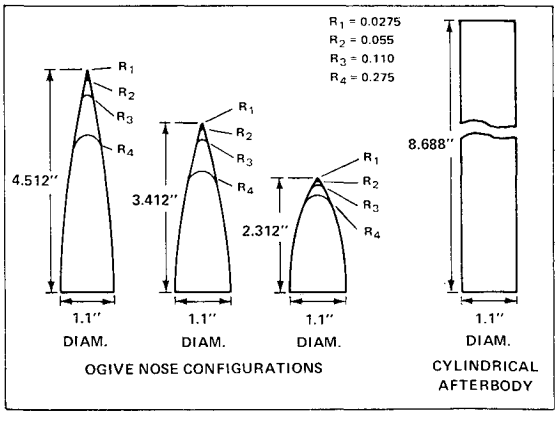

Fig. 1 Schematic diagram of test configurations.

Presented as Paper 71-570 at the AIAA 4th Fluid and Plasma Dynamics Conference, Palo Alto, Calif., June 21–23, 1971; synoptic received December 17, 1971; revision received March 6, 1972. Full paper is available from AIAA. Price: AIAA members, $1.50; nonmembers, $2.00, Microfiche, $1.00. **Order must be accompanied by remittance.**

Index categories: Subsonic and Transonic Flow; Uncontrolled Rocket and Missile Dynamics; Launch Vehicle and Missile Configuration Design.

* Aerospace Engineer. Member AIAA.

† Defined as $C_Y = Y/S_b q$ (Y, side force; q, dynamic pressure; S_b, base area).

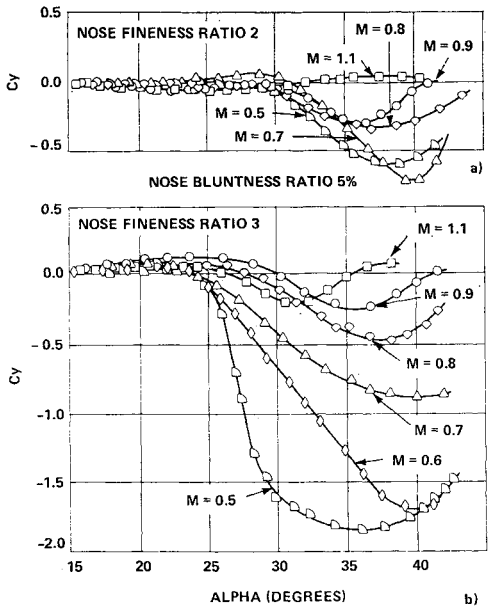

Fig. 2 Side force coefficient vs angle of attack at various Mach numbers and fineness ratios.

Increasing of the nose bluntness ratio beyond 20%, in general, reduces C_Y. This is evident if one compares Figs. 2b and 3b. The reduction is most pronounced for the lowest Mach number cases. Comparison of Figs. 2b and 4b demonstrates that blunting can reduce C_Y even in cases where the nose is more slender. The reduction of C_Y for large bluntness

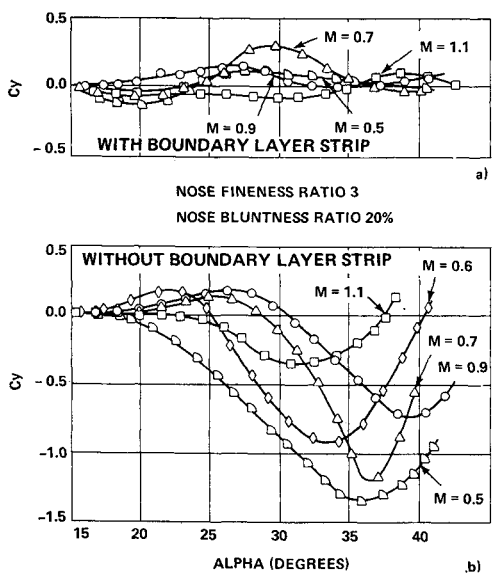

Fig. 3 Side force coefficient vs angle of attack at various Mach numbers with a) and without b) boundary-layer strip.

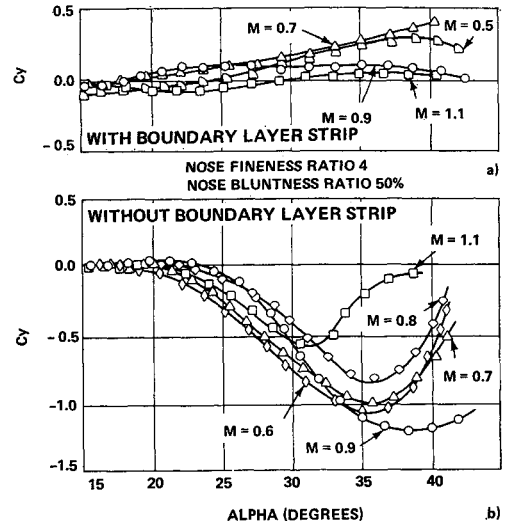

Fig. 4 Side force coefficient vs angle of attack at various Mach numbers with a) and without b) boundary layer-strip.

ratios may be explained on the basis that local laminar separation and reattachment bubbles form on the leeside with relatively high-local pressures, which causes a delay in the formation and subsequent detachment of the vortex sheets. This delay is sufficient for partial damping out of the initial nose tip disturbances and consequently, reducing the magnitude of C_Y.

The presence of a turbulent boundary layer considerably reduces the magnitude of C_Y. Figures 3 and 4 show this effect. This reduction, in most cases, amounted to no less than 50% and in certain instances as much as 80% in comparison to laminar boundary-layer results under identical test conditions. The physical reasons for the reduction in C_Y are connected to the observed reduction in the wake width and vortex strength relative to the laminar case.

On the basis of the above, consideration must be given to minimize C_Y when slender missile configurations are designed for high α and low Mach number conditions. The most effective way to achieve this is to use small fineness ratio or high-bluntness ratio noses and insure turbulent boundary layer on the surface.

References

[1] Carlyle, J. E., "Body Alone Characteristics at Angles of Attack," Independent Development Tactical Missile Maneuverability Study, Secs. 3.3 and 3.4 TM-55-21-92 LMSC/806605, May 1967, Lockheed Missiles & Space Co., Sunnyvale, Calif.

[2] Krouse, J. R., "Induced Side Forces on Slender Bodies at High Angles of Attack and Mach Numbers of 0.55 and 0.80," NSRDC Test Rept. AL-79, March 1971, Naval Ship Research and Development Center, Bethesda, Md.

[3] Thomson, K. D. and D. F. Morrison, "The Spacing, Position and Strength of Vortices in the Wake of Slender Cylindrical Bodies at Large Incidence," WRE TR NSA 25, June 1969, Weapons Research Establishment, Brisbane, Australia.